EVS27
Barcelona, Spain, November 17-20, 2013

Longitudinal and Lateral Coordinated Motion Control of Four-Wheel-Independent Drive Electric Vehicles

Yifan Dai, Yugong Luo, Keqiang Li
Tsinghua University, Beijing, China, dyf08@mails.tsinghua.edu.cn

Abstract

The movement of vehicle on the road can be divided into longitudinal motion and lateral motion. A coordinated longitudinal and lateral motion control system for four-wheel-independent drive electric vehicles (4WID EV) is proposed in order to improve the vehicle handling stability and energy efficiency. Using the information from GPS and INS, the state estimator is established to estimate longitudinal velocity and vehicle sideslip angle. The upper controller is used for tire force distribution based on the optimization of tire workload and energy dissipation. With the use of an inverse tire model, the lower controller is built for tire force control. The simulation and field test results show that the longitudinal and lateral coordinated motion control system can improve the vehicle handling stability and energy efficiency effectively.

Keywords: four-wheel independent drive; motion control; state estimation; tire force distribution; tire force control

1 Introduction

Electric vehicle industry is rapidly developing under the pressure of energy saving and environmental protection. As a promising type of electric vehicles[1], 4WID EV has more controllable dimensions than the centralized EV, which means greater potential to improve the vehicle performance[2].

Longitudinal and lateral coordinated motion control can improve the vehicle handling stability and energy efficiency while keeping the vehicle motion as driver desired. The existing researches mainly focus on the conventional ICE vehicles and centralized EV. For the coordinated longitudinal and lateral motion control of 4WID EV, there are some problems in the existing researches, such as the accuracy and robustness of the vehicle state estimation is not high enough, the performance index of tire force distribution is not optimal, and the accuracy of inverse tire model is limited.

Considering these problems, for the 4WID EV equipped with active front steering (AFS) system, a longitudinal and lateral coordinated motion control system is proposed. The key technologies, including vehicle state estimation, optimum tire force distribution and tire force control, are studied. Using the information from GPS/INS and combining the result of kinematic and dynamic method, the longitudinal velocity and vehicle sideslip angle are estimated. Tire workload and energy dissipation are used as the index of optimum tire force distribution in order to enhance the vehicle handling stability and energy efficiency respectively. Using an inverse tire model derived based on Dugoff model, the desired longitudinal and lateral tire forces are transformed to the desired tire slip ratio and tire sideslip angle, which are easier to observe and control. The effectiveness of the coordinated motion control system is verified through simulation and field test.

2 Hierarchical Control System

There are three key parts in a longitudinal and lateral coordinated motion control system: 1) Vehicle state estimator; 2) Allocation algorithm for longitudinal and lateral tire forces; 3) Execution control of longitudinal and lateral tire forces. Since the research objects and methods of these three parts are different, the hierarchical control structure is widely used[3,4]. In the hierarchical control structure, different control layers are linked with certain input and output signals, and the complexity of each control layer can be reduced.

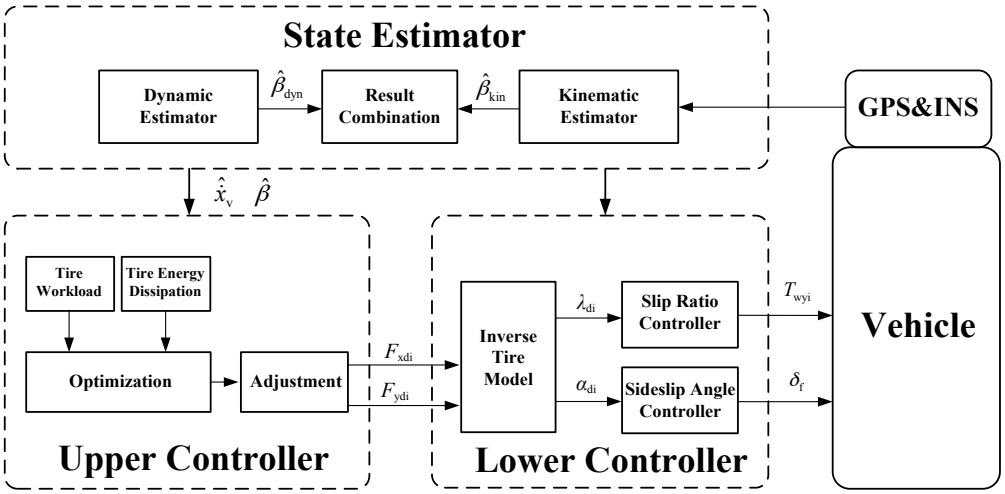

Figure 1: The hierarchical control structure

Figure 1 shows the proposed hierarchical control structure. Both the information from GPS and INS are used in the stated estimator to obtain the estimation of velocity and vehicle sideslip angle. A combination method between dynamic and kinematic estimators based on the error statistics is proposed. The upper controller is built for tire force distribution. Tire workload and energy dissipation are used as performance indexes. An adjustment method between these two indexes is proposed according to the driving condition. With an inverse tire model derived based on Dugoff tire model, the desired longitudinal and lateral tire forces from the upper controller are transformed to tire slip ratio and sideslip angle, which are easier to observe and control. Then the slip ratio and side slip angle controllers are established respectively in the lower controller.

3 State Estimator

In order to obtain the estimation of velocity and vehicle sideslip angle, both kinematic and dynamic methods are used in the state estimator. A result combination method based on the error statistics of the two estimators is proposed.

3.1 Kinematic Estimator

On a typical vehicle, there are in total three sets of frames: the East North Up frame (e-frame) for the GPS, the body frame (b-frame) for the INS and the ISO vehicle frame (v-frame) for the vehicle[5]. The relationship of these three frames is shown in figure2.

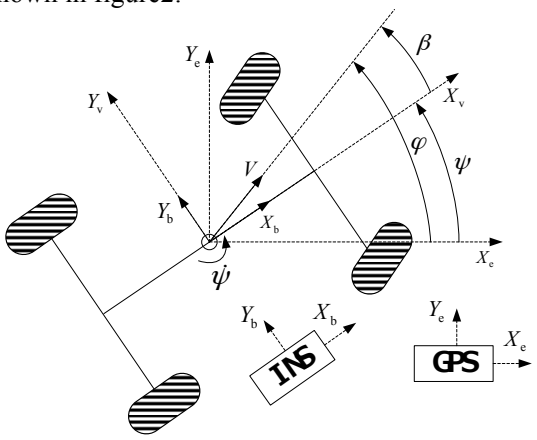

Figure 2: The relationship of different frames

Kalman filter uses only the last estimated value and the current observed value without the knowledge of the former values, which improves the real-time performance greatly. Two Kalman filters are established here to estimate the steady bias of yaw rate sensor and longitudinal/lateral accelerometers, details can be found in [6].

Kalman filter A - The correction of yaw rate sensor

$$\boldsymbol{x}_k^{(1)} = \boldsymbol{A}_1 \boldsymbol{x}_{k-1}^{(1)} + \frac{1}{2}\boldsymbol{B}_1(\boldsymbol{u}_k^{(1)} + \boldsymbol{u}_{k-1}^{(1)}) + \boldsymbol{w}_{k-1}^{(1)} \quad (1)$$

$$\boldsymbol{z}_k^{(1)} = \boldsymbol{H}_1 \boldsymbol{x}_k^{(1)} + \boldsymbol{v}_k^{(1)} \quad (2)$$

$$\boldsymbol{x}^{(1)} = \begin{bmatrix} \varphi & b_\psi \end{bmatrix}^{\mathrm{T}}, \quad \boldsymbol{u}^{(1)} = \dot{\psi}, \quad z^{(1)} = \varphi_{\mathrm{GPS}}$$

$$\boldsymbol{w}^{(1)} = \begin{bmatrix} -w_\psi \Delta t & w_{b_\psi} \dfrac{\Delta t}{T_{b_\psi}} \end{bmatrix}^{\mathrm{T}}, \quad \boldsymbol{v}^{(1)} = \varphi_{\mathrm{GPS}}^{\mathrm{error}}$$

$$\boldsymbol{A}_1 = \begin{bmatrix} 1 & -\Delta t \\ 0 & 1 - \dfrac{\Delta t}{T_{b_\psi}} \end{bmatrix}, \quad \boldsymbol{B}_1 = \begin{bmatrix} \Delta t & 0 \end{bmatrix}^{\mathrm{T}}, \quad \boldsymbol{H}_1 = [1 \quad 0]$$

Where b_ψ and w_ψ are the bias and noise of yaw rate sensor respectively, T_{b_ψ} is the Markov time constant for the bias, w_{b_ψ} is the Markov process noise, Δt is the sampling interval of GPS, $\boldsymbol{w}^{(1)}$ and $\boldsymbol{v}^{(1)}$ represent for the process noisy and measurement noisy respectively.

Kalman filter B - The correction of longitudinal /lateral accelerometers

$$\boldsymbol{x}_{\mathrm{k}}^{(2)} = \boldsymbol{A}_2 \boldsymbol{x}_{\mathrm{k-1}}^{(2)} + \frac{1}{2}\boldsymbol{B}_2 (\boldsymbol{u}_{\mathrm{k}}^{(2)} + \boldsymbol{u}_{\mathrm{k-1}}^{(2)}) + \boldsymbol{w}_{\mathrm{k-1}}^{(2)} \qquad (3)$$

$$\boldsymbol{z}_{\mathrm{k}}^{(2)} = \boldsymbol{H}_2 \boldsymbol{x}_{\mathrm{k}}^{(2)} + \boldsymbol{v}_{\mathrm{k}}^{(2)} \qquad (4)$$

$$\boldsymbol{x}^{(2)} = \begin{bmatrix} \dot{x}_{\mathrm{v}} & b_{\mathrm{x}} & \dot{y}_{\mathrm{v}} & b_{\mathrm{y}} \end{bmatrix}^{\mathrm{T}}, \quad \boldsymbol{u}^{(2)} = \begin{bmatrix} \ddot{x}_{\mathrm{b}} & \ddot{y}_{\mathrm{b}} \end{bmatrix}^{\mathrm{T}},$$

$$\boldsymbol{z}^{(2)} = \begin{bmatrix} V_{\mathrm{x}}^{\mathrm{GPS}} & V_{\mathrm{y}}^{\mathrm{GPS}} \end{bmatrix}^{\mathrm{T}}$$

$$\boldsymbol{w}^{(2)} = \begin{bmatrix} -w_{\mathrm{x}} \Delta t & w_{b_{\mathrm{x}}} \dfrac{\Delta t}{T_{b_{\mathrm{x}}}} & -w_{\mathrm{y}} \Delta t & w_{b_{\mathrm{y}}} \dfrac{\Delta t}{T_{b_{\mathrm{y}}}} \end{bmatrix}^{\mathrm{T}},$$

$$\boldsymbol{v}^{(2)} = [v_{\mathrm{GPS}} \quad v_{\mathrm{GPS}}]^{\mathrm{T}}$$

$$\boldsymbol{A}_2 = \begin{bmatrix} 1 & -\Delta t & \hat{\dot{\psi}} \Delta t & 0 \\ 0 & 1 - \dfrac{\Delta t}{T_{b_{\mathrm{x}}}} & 0 & 0 \\ -\hat{\dot{\psi}} \Delta t & 0 & 1 & -\Delta t \\ 0 & 0 & 0 & 1 - \dfrac{\Delta t}{T_{b_{\mathrm{y}}}} \end{bmatrix},$$

$$\boldsymbol{B}_2 = \begin{bmatrix} \Delta t & 0 \\ 0 & 0 \\ 0 & \Delta t \\ 0 & 0 \end{bmatrix}, \quad \boldsymbol{H}_2 = \begin{bmatrix} 1 & 0 & 0 & 0 \\ 0 & 0 & 1 & 0 \end{bmatrix}$$

Where $\hat{\dot{\psi}}$ is the corrected yaw rate, b_{x} and w_{x} are the bias and noise of longitudinal accelerometer, $T_{b_{\mathrm{x}}}$ is the Markov time constant for the bias, $w_{b_{\mathrm{x}}}$ is the Markov process noise. b_{y} and w_{y} are the bias and noise of lateral accelerometer, $T_{b_{\mathrm{y}}}$ is the Markov time constant for the bias, $w_{b_{\mathrm{y}}}$ is the Markov process noise.

Then the velocities in the v-frame can be calculated as Eq. (5) (6).

$$\hat{\dot{x}}_{\mathrm{v}} = V_{\mathrm{x}}^{\mathrm{GPS}} + \int_0^t \left(\hat{\ddot{x}}_{\mathrm{b}} + \hat{\dot{\psi}} \hat{\dot{y}}_{\mathrm{v}} \right) \mathrm{d}t \qquad (5)$$

$$\hat{\dot{y}}_{\mathrm{v}} = V_{\mathrm{y}}^{\mathrm{GPS}} + \int_0^t \left(\hat{\ddot{y}}_{\mathrm{b}} - \hat{\dot{\psi}} \hat{\dot{x}}_{\mathrm{v}} \right) \mathrm{d}t \qquad (6)$$

Where $V_{\mathrm{x}}^{\mathrm{GPS}}$ and $V_{\mathrm{y}}^{\mathrm{GPS}}$ are the longitudinal and lateral velocity from GPS at the sampling point, $\hat{\ddot{x}}_{\mathrm{b}}$ and $\hat{\ddot{y}}_{\mathrm{b}}$ are the corrected longitudinal and lateral acceleration.

The vehicle sideslip angle can be known as Eq. (7).

$$\beta = \arctan(\dot{y}_{\mathrm{v}} / \dot{x}_{\mathrm{v}}) \qquad (7)$$

3.2 Dynamic Estimator

The dynamic estimator is established based on UPF (Unscented Particle Filter), details can be found in [7].

The process equation is shown as Eq. (8).

$$\dot{\boldsymbol{x}}(t) = \boldsymbol{f}(\boldsymbol{x}(t), \boldsymbol{u}(t)) \qquad (8)$$

where

$$\boldsymbol{u} = \begin{bmatrix} \delta & F_{\mathrm{x1}} & F_{\mathrm{x2}} & F_{\mathrm{x3}} & F_{\mathrm{x4}} \end{bmatrix}^{\mathrm{T}}$$

$$\boldsymbol{x} = \begin{bmatrix} v_{\mathrm{x}} & v_{\mathrm{y}} & \dot{\psi} & F_{\mathrm{y1}} & F_{\mathrm{y2}} & F_{\mathrm{y3}} & F_{\mathrm{y4}} \end{bmatrix}^{\mathrm{T}}$$

δ is the steering wheel angle, F_{xi} and F_{yi} are the longitudinal and lateral force of wheel i, v_{x} and v_{y} are the longitudinal and lateral velocity.

The measurement equation is shown as Eq. (9).

$$\boldsymbol{z}(t) = \boldsymbol{h}(\boldsymbol{x}(t), \boldsymbol{u}(t)) \qquad (9)$$

where

$$\boldsymbol{z} = \begin{bmatrix} \ddot{x}_{\mathrm{bm}} & \ddot{y}_{\mathrm{bm}} & \dot{\psi}_{\mathrm{m}} & \omega_1 & \omega_2 & \omega_3 & \omega_4 \end{bmatrix}^{\mathrm{T}}$$

$\ddot{x}_{\mathrm{bm}}$, $\ddot{y}_{\mathrm{bm}}$ and $\dot{\psi}_{\mathrm{m}}$ are the measurement of longitudinal/lateral accelerometer and yaw rate sensor respectively, ω_{i} is the rotation speed of wheel i.

3.3 Result Combination

The kinematic estimator is highly dependent on the accuracy of sensors. With the increase of velocity and accelerations, the signal to noise ratio (SNR) of the sensors increase, so the accuracy of the kinematic estimator enhances. On the other hand, with the increase of velocity and accelerations, the nonlinearity of the vehicle increases, which leads to the model mismatch in the dynamic estimator.

According to the complementary characteristics of these two estimators, a result combination method is proposed to enhance the accuracy of vehicle sideslip angle, as shown in Eq. (10).

$$\hat{\beta} = \frac{\sigma_{\mathrm{dyn}}^2}{\sigma_{\mathrm{kin}}^2 + \sigma_{\mathrm{dyn}}^2} \hat{\beta}_{\mathrm{kin}} + \frac{\sigma_{\mathrm{kin}}^2}{\sigma_{\mathrm{kin}}^2 + \sigma_{\mathrm{dyn}}^2} \hat{\beta}_{\mathrm{dyn}} \qquad (10)$$

Where $\hat{\beta}_{\mathrm{kin}}$ and $\hat{\beta}_{\mathrm{dyn}}$ are the estimation of vehicle sideslip angle in kinematic and dynamic estimator respectively. σ_{kin} and σ_{dyn} are the statistical estimation error of these two methods, which are described as the function of road friction coefficient μ and vehicle lateral acceleration a_{y}, as shown in Eq. (11) and (12).

$$\sigma_{\mathrm{kin}} = f_{\mathrm{kin}}(\mu, a_{\mathrm{y}}) \qquad (11)$$

$$\sigma_{dyn} = f_{dyn}(\mu, a_y) \quad (12)$$

The theoretical value of estimation error in Eq. (10) is calculated as Eq. (13).

$$\hat{\sigma}^2 = \frac{\sigma_{kin}^2 \sigma_{dyn}^2}{\sigma_{kin}^2 + \sigma_{dyn}^2} \le \min(\sigma_{kin}^2, \sigma_{dyn}^2) \quad (13)$$

The theoretical value of estimation error after result combination is lower than the error in the two estimators.

4 Upper Controller

In the upper controller, the longitudinal forces of four wheels and the lateral forces of the front wheels are optimally distributed in order to improve certain vehicle performance. To enhance the stability performance, the cost function based on minimizing the variance and mean value of tire workload is proposed. To improve the economy performance, the cost function based on tire energy dissipation is used.

Based on the planar vehicle model in figure 3, the driver's manoeuvre intention are considered as constraints, as shown in Eq. (14)-(16), where F_{yf} is the total lateral force of the front wheels, F_{xd}, F_{yd} and M_d are the desired total longitudinal tire force, lateral tire force and yaw moment respectively.

$$F_{x1} + F_{x2} + F_{x3} + F_{x4} = F_{xd} \quad (14)$$

$$F_{yf} + F_{y3} + F_{y4} = F_{yd} \quad (15)$$

$$\frac{t_w}{2}(F_{x2} - F_{x1} + F_{x4} - F_{x3}) + l_f F_{yf} - l_r(F_{y3} + F_{y4}) = M_d \quad (16)$$

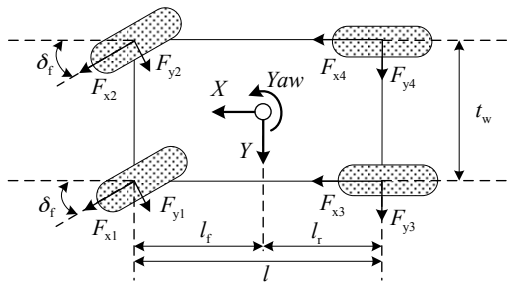

Figure 3: Planar vehicle model

4.1 Tire Force Distribution Based on Tire Workload

Tire workload γ is defined as Eq. (17), where F_{zi} is the vertical load on tire i, μ_i is the friction coefficient between road and tire i.

$$\gamma_i = \frac{F_{xi}^2 + F_{yi}^2}{\mu_i^2 F_{zi}^2} \quad (17)$$

Both the method of minimizing the sum of tire workload[8] and minimizing the variance of tire workload[9] are studied by different researchers. Considering the shortage of these two methods, the cost function based on minimizing the variance and mean value of tire workload is proposed, as shown in Eq. (18), where ε_v is the weight coefficient between variance and mean value.

$$\min\ J = \mathrm{Var}(\gamma_i) + \varepsilon_v \mathrm{E}(\gamma_i) = \frac{1}{4}\sum_{i=1}^{4}(\gamma_i - \mathrm{E}(\gamma_i))^2 + \varepsilon_v \mathrm{E}(\gamma_i) \quad (18)$$

This kind of cost function can reduce both the variance and mean value of tire workload. The adhesion potential of each tire is fully used. The vehicle stability performance can be improved significantly.

4.2 Tire Force Distribution Based on Tire Energy Dissipation

Tire energy dissipation represents the energy loss due to the friction between tire and road. Energy dissipation Q can be calculated by the integration of dissipation power P, as shown in Eq. (19), where v_{rx} and v_{ry} are the longitudinal and lateral relative velocity between tire and road.

$$Q = \int P \mathrm{d}t = \int (v_{rx} F_x + v_{ry} F_y) \mathrm{d}t \quad (19)$$

The longitudinal and lateral relative velocity between tire and road can be calculated as Eq. (20) and (21), where V is the velocity of the vehicle, ω is the rotation speed of the wheel, and α is the sideslip angle of the tire.

$$v_{rx} = \omega R - V\cos\alpha \quad (20)$$

$$v_{ry} = -V\cos\alpha \quad (21)$$

The cost function based on the optimization of tire energy dissipation is established as a standard quadratic form, as shown in Eq. (22).

$$\min\ J = \frac{1}{2}\boldsymbol{X}^{\mathrm{T}}\boldsymbol{H}_d\boldsymbol{X} \quad (22)$$

Where $\boldsymbol{X} = \begin{bmatrix} F_{x1} & F_{x2} & F_{x3} & F_{x4} & F_{yf} \end{bmatrix}^{\mathrm{T}}$

$$\boldsymbol{H}_d = 2\begin{bmatrix} v_{rx1}^2 & 0 & 0 & 0 & 0 \\ 0 & v_{rx2}^2 & 0 & 0 & 0 \\ 0 & 0 & v_{rx3}^2 & 0 & 0 \\ 0 & 0 & 0 & v_{rx4}^2 & 0 \\ 0 & 0 & 0 & 0 & v_{ry1}^2\varepsilon_f^2 + v_{ry2}^2(1-\varepsilon_f)^2 \end{bmatrix}$$

ε_f is the distribution coefficient of lateral forces between front left wheel and front right wheel.

4.3 Dynamic Adjustment of the Optimization Results

The cost functions of tire workload and energy dissipation represent the optimization of vehicle stability and economy respectively. The optimization results should be adjusted according to the vehicle state in order to improve the vehicle performance in different conditions.

According to the tire brush model, the lateral tire force reaches the nonlinear region when:

$$F_y \geq 0.58\mu F_z \quad (23)$$

Define the lateral acceleration coefficient as:

$$a_{yr} = a_y / \mu g \quad (24)$$

According to Eq. (23), the tire lateral force reaches the nonlinear region when:

$$a_{yr} \geq 0.58 \quad (25)$$

Eq. (25) includes the affect of both lateral acceleration and road adhesion situation on vehicle stability, and can be used as an index of vehicle stability state.

The velocity is another important index of vehicle stability state. Taking both normalized lateral acceleration and velocity into account, the dynamic adjustment of the optimization results can be expressed as Eq. (26).

$$\boldsymbol{F} = \varepsilon_d \boldsymbol{F}_w + (1-\varepsilon_d)\boldsymbol{F}_d \quad (26)$$

Where $\boldsymbol{F}_w$ and $\boldsymbol{F}_d$ represent the force distribution results based on tire workload and energy dissipation respectively, ε_d is the weight coefficient between these two methods, which is calculated by the normalized lateral acceleration and velocity, as shown in figure 4.

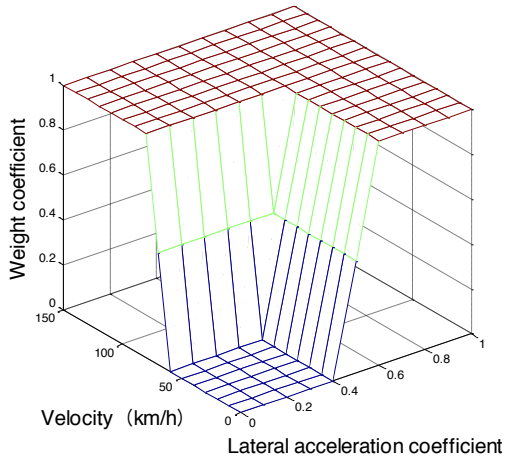

Figure: 4 Weight coefficient

5 Lower Controller

In the lower controller, the desired longitudinal and lateral tire forces are transformed to the desired tire slip ratio and sideslip angle through an inverse tire model. Compared to the longitudinal and lateral tire force, the tire slip ratio and sideslip angle are easier to estimate and control. Then the slip ratio controller and sideslip angle controller are established based on sliding mode control and feedforward/feedback combined control respectively.

5.1 Inverse Tire Model

Dugoff tire model has been widely used because of its high accuracy and the concise form, as shown in Eq. (27).

$$\begin{cases} F_x = C_\lambda \dfrac{\lambda}{1+\lambda} f(H_D) \\ F_y = C_\alpha \dfrac{\tan\alpha}{1+\lambda} f(H_D) \end{cases} \quad (27)$$

Where C_λ and C_α are the longitudinal slip stiffness and cornering stiffness of the tire respectively.

$$f(H_D) = \begin{cases} (2-H_D)H_D, & H_D < 1 \\ 1, & H_D \geq 1 \end{cases} \quad (28)$$

$$H_D = \frac{\mu F_z (1+\lambda)}{2\sqrt{(C_\lambda \lambda)^2 + (C_\alpha \tan\alpha)^2}} \quad (29)$$

Here tire slip ratio λ is defined as Eq. (30).

$$\lambda = \begin{cases} \dfrac{\omega R - V}{\omega R} & (V - \omega R \leq 0) \\ \dfrac{\omega R - V}{V} & (V - \omega R > 0) \end{cases} \quad (30)$$

Based on Dugoff tire model, an inverse tire model is derived as shown in Eq. (31) and (32).

$$\lambda = \begin{cases} \dfrac{F_x}{C_\lambda - F_x} & (D \geq 1) \\ \dfrac{\mu^2 F_x F_z^2}{4C_\lambda \sqrt{F_x^2 + F_y^2}(\mu F_z - \sqrt{F_x^2 + F_y^2}) - \mu^2 F_x F_z^2} & (D < 1) \end{cases} \quad (31)$$

$$\alpha = \begin{cases} \tan^{-1} \dfrac{F_y C_\lambda}{C_\alpha (C_\lambda - F_x)} & (D \geq 1) \\ \tan^{-1} \dfrac{C_\lambda \mu^2 F_y F_z^2}{4C_\lambda C_\alpha \sqrt{F_x^2 + F_y^2}(\mu F_z - \sqrt{F_x^2 + F_y^2}) - C_\alpha \mu^2 F_x F_z^2} & (D < 1) \end{cases} \quad (32)$$

Where D is defined as Eq. (33).

$$D = \frac{\mu F_z}{2\sqrt{F_x^2 + F_y^2}} \quad (33)$$

Using this inverse tire model, the desired longitudinal and lateral tire force can be transformed to the desired tire slip ratio and sideslip angle, which are easier to estimate and control.

5.2 Tire Slip Ratio Control

The sliding mode control method is chosen here for tire slip ratio control because of its robustness against uncertainty. A quarter vehicle model, as shown in figure 5 and described by Eq. (34) and (35), is used for the controller design.

$$m_q \dot{V} = F_x - \frac{1}{2}\rho C A_q V^2 \quad (34)$$

$$J_w \dot{\omega} = T_{wy} - F_x R \quad (35)$$

The longitudinal tire force can be described as:

$$F_x = \kappa(\lambda) mg \quad (36)$$

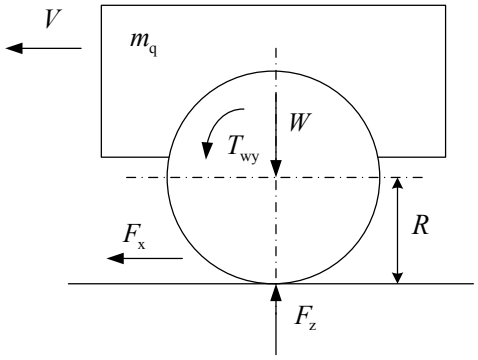

Figure: 5 Quarter vehicle model

Where $\kappa(\lambda)$ represents the friction coefficient at tire slip ratio λ. The derivative form of Eq. (36) can be described as:

$$\dot{\lambda}=\begin{cases}\dfrac{V}{\omega^2 R}\dot{\omega}-\dfrac{\dot{V}}{\omega R} & (\lambda\geq 0)\\ -\dfrac{\omega R}{V^2}\dot{V}+\dfrac{\dot{\omega}R}{V} & (\lambda<0)\end{cases} \tag{37}$$

The nonlinear system for tire slip ratio control can be described as:

$$\begin{cases}\dot{x}_1=a_{11}x_1^2+\kappa(x_3)g\\ \dot{x}_2=a_{21}\kappa(x_3)+a_{22}T_{wy}\\ \dot{x}_3=f_{31}(x_1,x_2)+f_{32}(x_1,x_2)\kappa(x_3)+f_{33}(x_1,x_2)T_{wy}\end{cases} \tag{38}$$

Where $X=[x_1,x_2,x_3]^T=[V,\omega,\lambda]^T$, $a_{11}=-\rho CA/m$, $a_{21}=-mgr/J_w$, $a_{22}=1/J_w$

$$f_{31}(x_1,x_2)=\begin{cases}-a_{11}x_1^2/Rx_2 & x_3\geq 0\\ -a_{11}Rx_2 & x_3<0\end{cases}$$

$$f_{32}(x_1,x_2)=\begin{cases}(-g/Rx_2+a_{21}x_1/Rx_2^2) & x_3\geq 0\\ a_{21}R/x_1-gRx_2/x_1^2 & x_3<0\end{cases}$$

$$f_{33}(x_1,x_2)=\begin{cases}a_{22}x_1/Rx_2^2 & x_3\geq 0\\ a_{22}R/x_1 & x_3<0\end{cases}$$

The siding surface is chosen as:

$$S=c_1e_w+c_2\int e_w\mathrm{d}t \tag{39}$$

Where e_w is the error between desired slip ratio and actual slip ratio, c_1 and c_2 are the adjustable parameters of the siding surface. The reaching rate is chosen as:

$$\dot{S}=-k_pS-k_s\cdot\mathrm{sgn}(S) \tag{40}$$

The driving toque calculated by the sliding mode controller can be described as Eq. (41).

$$T_{wy}=\frac{\ddot{\lambda}_d-f_{31}-f_{32}\kappa(\lambda)-c_3e_w-c_4\int e_w\mathrm{d}t-k_s\,\mathrm{sgn}(S)/c_1}{f_{33}} \tag{41}$$

Where $c_3=(c_2+k_pc_1)/c_1$, $c_4=k_pc_2/c_1$

5.3 Tire Sideslip Angle Control

Based on the single-track vehicle model, the desired tire sideslip angle can be transformed to the desired steering angle of front wheels, as shown in Eq. (42).

$$\delta_d=\beta+\frac{l_f\dot{\gamma}}{V}-\alpha_d \tag{42}$$

The feedforward and feedback compensators are established for the control of steering angle. For the feedforward compensator, the steering motor torque T_{mf} is obtained based on the estimation of tire aligning torque and the calculation of the inertia and damping of the steering system, as shown in Eq. (43).

$$T_{mf}=(\frac{T_a}{G_s}+T_e)/G_m \tag{43}$$

Where T_a is the aligning torque of the tire, G_s is the transmission ratio of the steering system, T_e is the torque to overcome the effect of inertia and damping of the steering system, G_m is the transmission ratio between steering motor and steering column.

For the feedback compensator, the PID control method is used to calculate the steering motor torque T_{mb}, as shown in Eq. (44).

$$T_{mb}=K_Pe_\delta+K_I\int_0^t e_\delta\mathrm{d}t+K_D\frac{\mathrm{d}e_\delta}{\mathrm{d}t} \tag{44}$$

Where e_δ is the error between the desired steering angle and the actual steering angle. The torque of the steering motor is obtained as Eq. (45).

$$T_m=T_{mf}+T_{mb} \tag{45}$$

6 Simulation Result

The simulation system is established based on MSC CarSim and Matlab/Simulink. The proposed coordinated motion control system is verified through simulation.

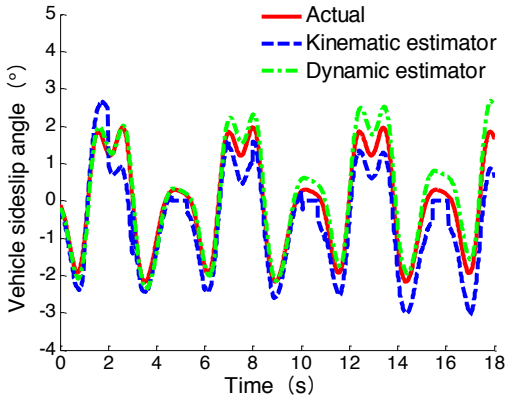

Figure: 6 Estimation results of different estimators

Figure 6 shows the vehicle sideslip angle estimation results of two estimators in continuous double lane change. The RMS error of kinematic and dynamic estimators are 0.63° and 0.26° respectively. Figure 7 shows the result after combination of the two estimators. The

combination result is closer to the actual value compared to the kinematic and dynamic estimator, the RMS error reduces to 0.20°

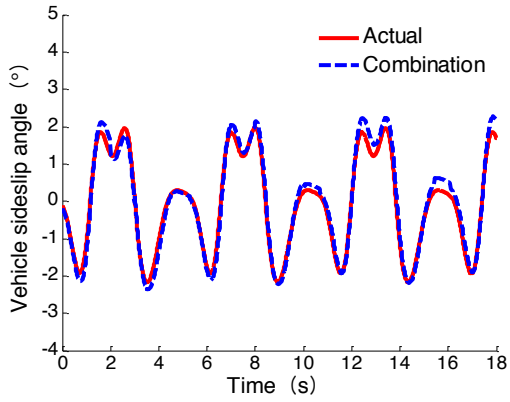

Figure: 7 Combination result

Figure 8 and figure 9 show the result of vehicle sideslip angle and vehicle trace in double lane change when using the optimization of tire workload. The sideslip angle of the vehicle with tire workload control is smaller than the one without control. In figure 9, the vehicle with tire workload control also shows a better stability performance.

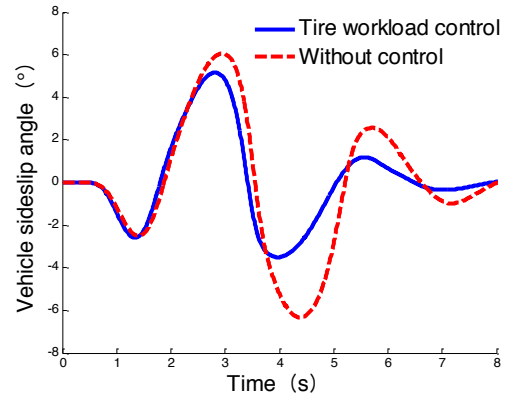

Figure: 8 Comparison of vehicle sideslip angle

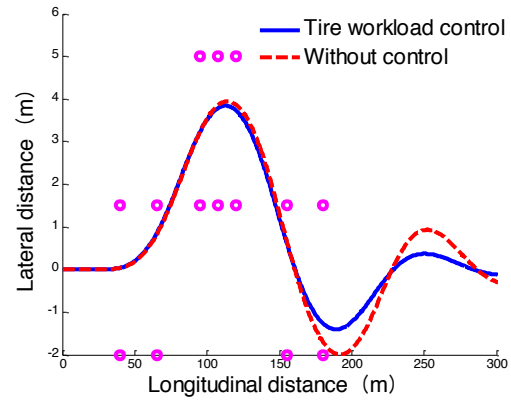

Figure: 9 Comparison of vehicle trace

Figure 10 shows the optimization result of tire energy dissipation in a double lane change. Compare to the results in workload control and no control, the dissipation control can reduce the tire energy dissipation significantly.

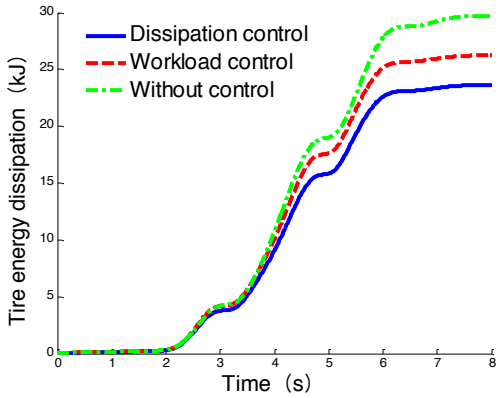

Figure: 10 Tire energy dissipation

7 Field Test

To verify the proposed coordinated motion control system, a four-wheel-independent drive electric vehicle is built based on BJ JEEP 2023. Figure 11 (a) shows chassis structure of the test vehicle and Figure 11 (b) is the outward appearance.

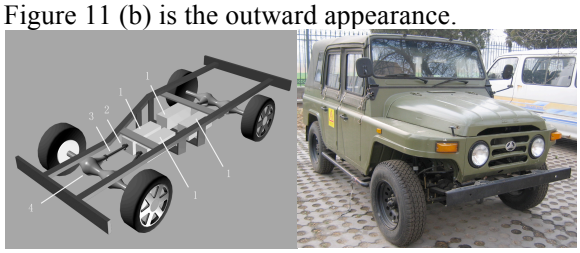

(a) Chassis structure (b) Outward appearance

Figure 11 The 4WID EV

1-Motor; 2- Universal joint; 3-Drive shaft; 4-Main reducer

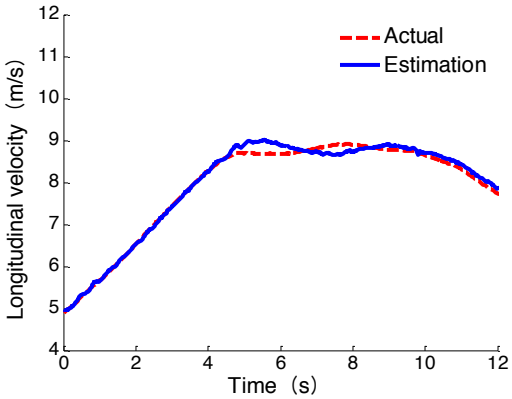

Figure: 12 Estimation of longitudinal velocity

Figure 12 and 13 show the estimation results of longitudinal velocity and vehicle sideslip angle in a double lane change test. The RMS error and max error of longitudinal velocity are 0.13m/s and 0.35m/s respectively. For the estimation of vehicle sideslip angle, the errors are 0.25° and 0.93°.

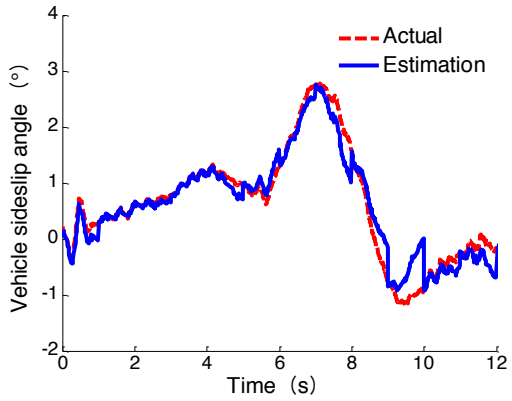

Figure: 13 Estimation of vehicle sideslip angle

The tire workload optimization method is verified on the icy road. The test vehicle drives straight on the road. For comparison, in the no control group, the motor driving torque is evenly distributed. Figure 14 and figure 15 show the comparison of the accelerator pedal position and the longitudinal acceleration with and without control. The vehicle with control has bigger pedal opening and reaches greater acceleration than the vehicle without control.

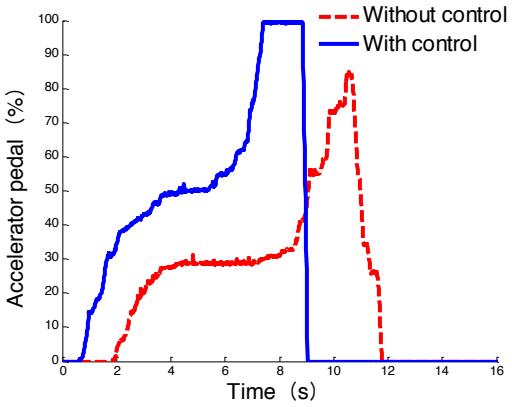

Figure: 14 Accelerator pedal

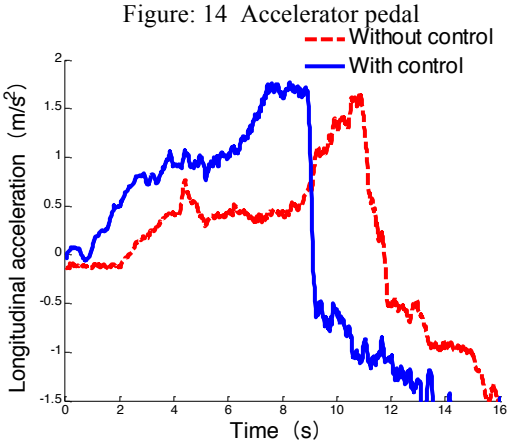

Figure: 15 Longitudinal acceleration

Figure 16 and figure 17 show the wheel edge velocity of vehicle with and without control. In figure 16, the FL and FR wheel of the vehicle start to slip at about the 10ths, while in figure 17, all the wheels are controlled well without slip.

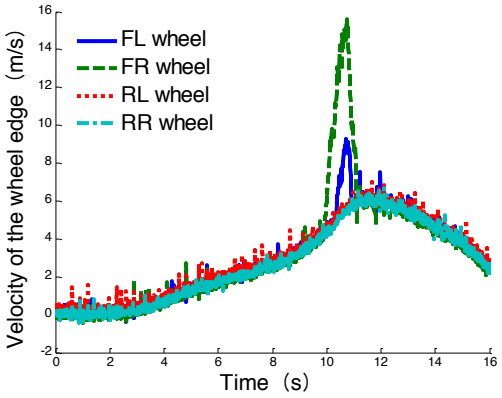

Figure: 16 Wheel speed (without control)

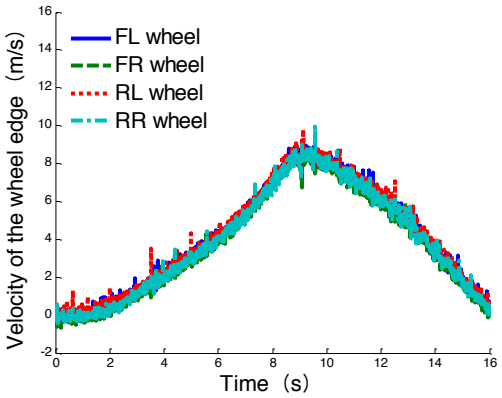

Figure: 17 Wheel speed (with control)

The field test result verifies that the coordinated motion control system can prevent the vehicle from slip, and improve the handling stability.

8 Conclusion

A longitudinal and lateral coordinated motion control system for 4WID EV with AFS is proposed, the method for vehicle state estimation, tire force distribution and tire force control are studied.

To estimate the longitudinal velocity and vehicle sideslip angle, the information from both GPS and INS are used. A combination method between dynamic and kinematic estimators based on the error statistics is proposed. Tire workload and energy dissipation are chosen as performance index for the tire force distribution. A dynamic adjustment method is proposed to choose the suitable optimization result according to the vehicle state. The desired longitudinal and lateral tire forces are then transformed to the desired tire slip ratio and sideslip angle, which are easier to observe and control. Then the tire slip ratio and sideslip angle controller are established respectively. The simulation and field test results

verify that the longitudinal and lateral coordinated motion control system can improve the vehicle handling stability and energy efficiency effectively.

Acknowledgments

This work was supported by the National Key Fundamental Research Program of China-973 Program (2011CB711204); the MOST (Ministry of Science and Technology) of China under the contract of No.2010DFA72760.

References

[1] Satoshi Murata, *Innovation by in-wheel-motor drive unit,* Vehicle System Dynamics, Vol. 50, No. 6, p.807-830, 2012.

[2] Wenbo Chu, Yugong Luo, Yifan Dai, et al., *Traction Fault Accommodation System for Four Wheel Independently Driven Electric Vehicle,* EVS26, Los Angeles, USA, 2012.

[3] Daofei Li, Shangqian Du, Fan Yu, *Integrated vehicle chassis control based on direct yaw moment, active steering and active stabilizer,* Vehicle System Dynamics, Vol. 46, No. 1, p.341 -351, 2008.

[4] Wanki Cho, JangyeolYoon, Jeongtae Kim, et al., *An investigation into unified chassis control scheme for optimised vehicle stability and manoeuvrability,* Vehicle System Dynamics, Vol. 46, No. 1, p.87 - 105, 2008.

[5] K. Tin Leung, J. F. Whidborne , D. Purdy, et al., *A review of ground vehicle dynamic state estimations utilising GPS/INS,* Vehicle System Dynamics, Vol. 49, No. 1, p.29–58, 2011.

[6] Yifan Dai, Yugong Luo, Wenbo Chu, et al., *Vehicle State Estimation Based on Integration of Low-Cost GPS and INS,* International Conference on Advanced Vehicle Technologies and Integration, Changchun, China, 2012.

[7] Wenbo Chu, Yugong Luo, Yifan Dai, et al., *Vehicle State Estimation for In-Wheel Motor Electric Vehicle Using Unscented Particle Filter,* International Conference on Advanced Vehicle Technologies and Integration, Changchun, China, 2012.

[8] Ossama Mokhiamar, Masato Abe, *How the four wheels should share forces in an optimum cooperative chassis control,* Control Engineering Practice, Vol. 14, p.295-304, 2006.

[9] Huei Peng, Rahman Sabahi, Shih-Ken Chen, et al., *Integrated Vehicle Control Based on Tire Force Reserve Optimization Concept,* ASME International Mechanical Engineering Congress and Exposition, Denver, USA, 2011.

Authors

Yifan Dai received the Ph.D. and Bachelor degrees from Tsinghua University, Beijing, China, in 2013 and 2008 respectively. He is currently a post-doctor at the Department of Automotive Engineering, Tsinghua University. His research interests include advanced active safety control and electric vehicle control.

Yugong Luo received the Ph.D. degree from Tsinghua University, Beijing, China, in 2003, and the Master and Bachelor degrees from Chongqing University, Chongqing, China, in 1999 and 1996 respectively. He is currently an Associate Professor with the Department of Automotive Engineering, Tsinghua University, Beijing, China. His active research interests include Vehicle & EV dynamics and control, and Vehicle NVH analysis and control.

Keqiang Li received Ph.D. and Master degrees from Chongqing University in 1995 and 1988 respectively, and the Bachelor degree from Tsinghua University in 1985. He is currently a Professor with the Department of Automotive Engineering, Tsinghua University. His main areas of research interest include vehicle dynamics and control for driver assistance systems and hybrid electrical vehicles.